ELSEVIER

Nuclear Engineering and Design 187 (1999) 277–290

Nuclear Engineering and Design

Modified crack closure integral based computation of stress intensity factors for 2-D thermoelastic problems through boundary element method

N.K. Mukhopadhyay [a,1], S.K. Maiti [b,*], A. Kakodkar[a,1]

[a] *Reactor Design and Development Group, Bhabha Atomic Research Centre, Mumbai 400085, India*
[b] *Department of Mechanical Engineering, Indian Institute of Technology, Bombay, Mumbai 400076, India*

Received 1 January 1998; received in revised form 25 August 1998; accepted 23 November 1998

Abstract

A modified crack closure integral (MCCI) based computation of stress intensity factors (SIFs) for thermal loading through boundary element method (BEM) is presented. Simple relations are given for the determination of stress intensity factors (SIFs) using the BEM results for linear, quadratic and quarter point elements employed around the crack tip. Examples of crack under mode I, mode II and mixed mode thermal and/or mechanical loading are examined. The computed SIFs are compared wherever possible with solutions available in the literature. The agreement is good. The effect of crack tip element size on the accuracy of results is reported.

1. Introduction

The stress intensity factors (SIFs) for thermal problems can be determined through the boundary element method (BEM) using the formulation presented by Rizzo and Shippy (1977). A number of studies involving thermal loading of a crack, e.g. Lee and Cho (1990), Raveendra and Banerjee (1992), Raveendra et al. (1993), Prasad et al. (1994, 1996), Sladek and Sladek (1993, 1997), Katsareas and Anifantis (1995), etc. has been reported. The thermoelastic boundary element (BE) formulation coupled with either the subregion analysis (Blandford et al., 1981), or the dual boundary element method (DBEM) (Portela et al., 1992) has extended the scope of analysis to mixed mode fracture problems. The subregion analysis is simpler than the DBEM and has been applied by a number of investigators, e.g. Raveendra and Banerjee (1992), Raveendra et al. (1993), Katsareas and Anifantis (1995), etc. In the DBEM, the singularity in the final system of equations is avoided by using two different equations for the boundary nodes on the opposite crack edges. For the thermoelastic crack problems, displacement and temperature equations are specified on one crack edge and the traction and

* Corresponding author. Tel.: +91-22-5767526; fax: +91-22-5783480; e-mail: skmaiti@me.iitb.ernet.in.

[1] Tel.: +91-22-5505050, extn. 2586; fax: +91-22-5505151; e-mail:nirmalk@apsara.barc.ernet.in

0029-5493/99/$ - see front matter
PII: S0029-5493(98)00304-5

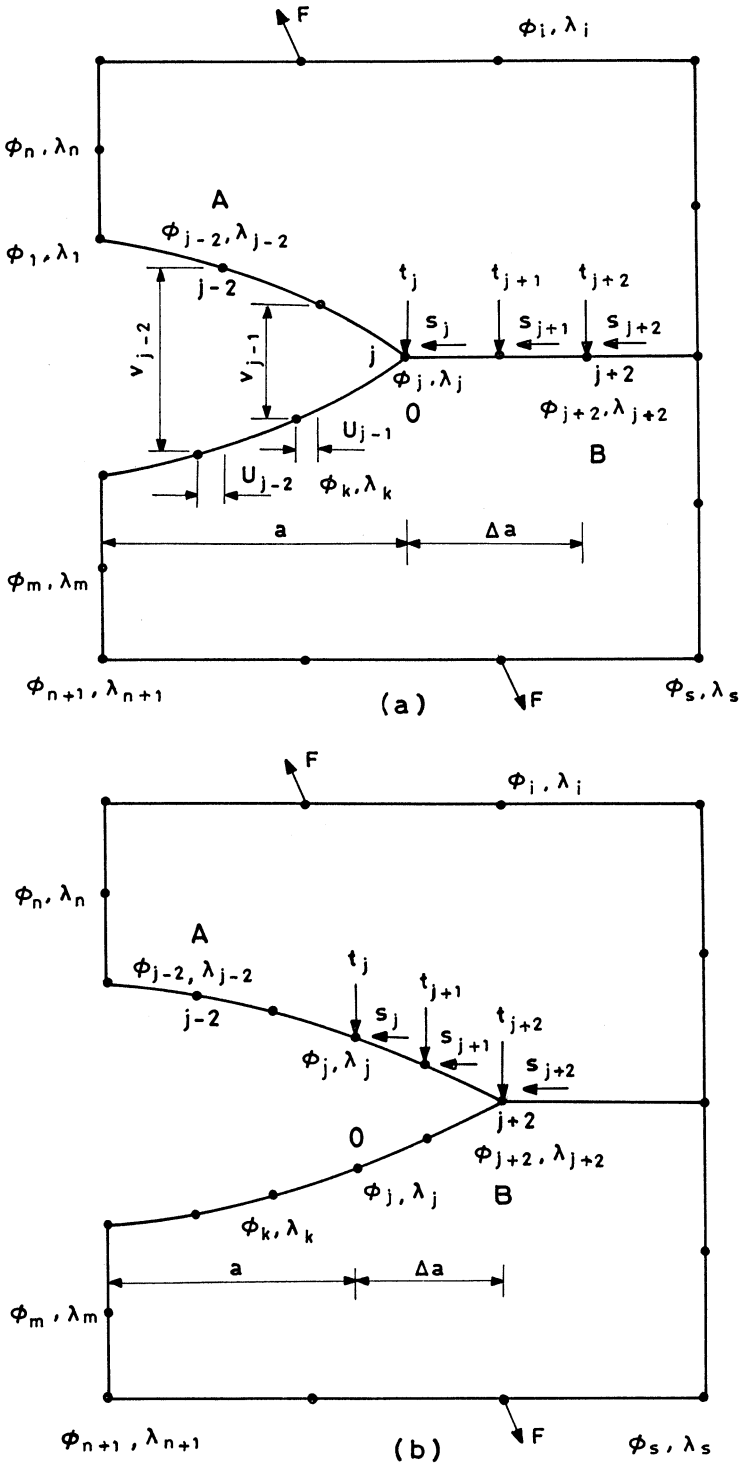

Fig. 1. Illustration of (a) crack under remote mechanical loading and thermal field and (b) crack closure forces.

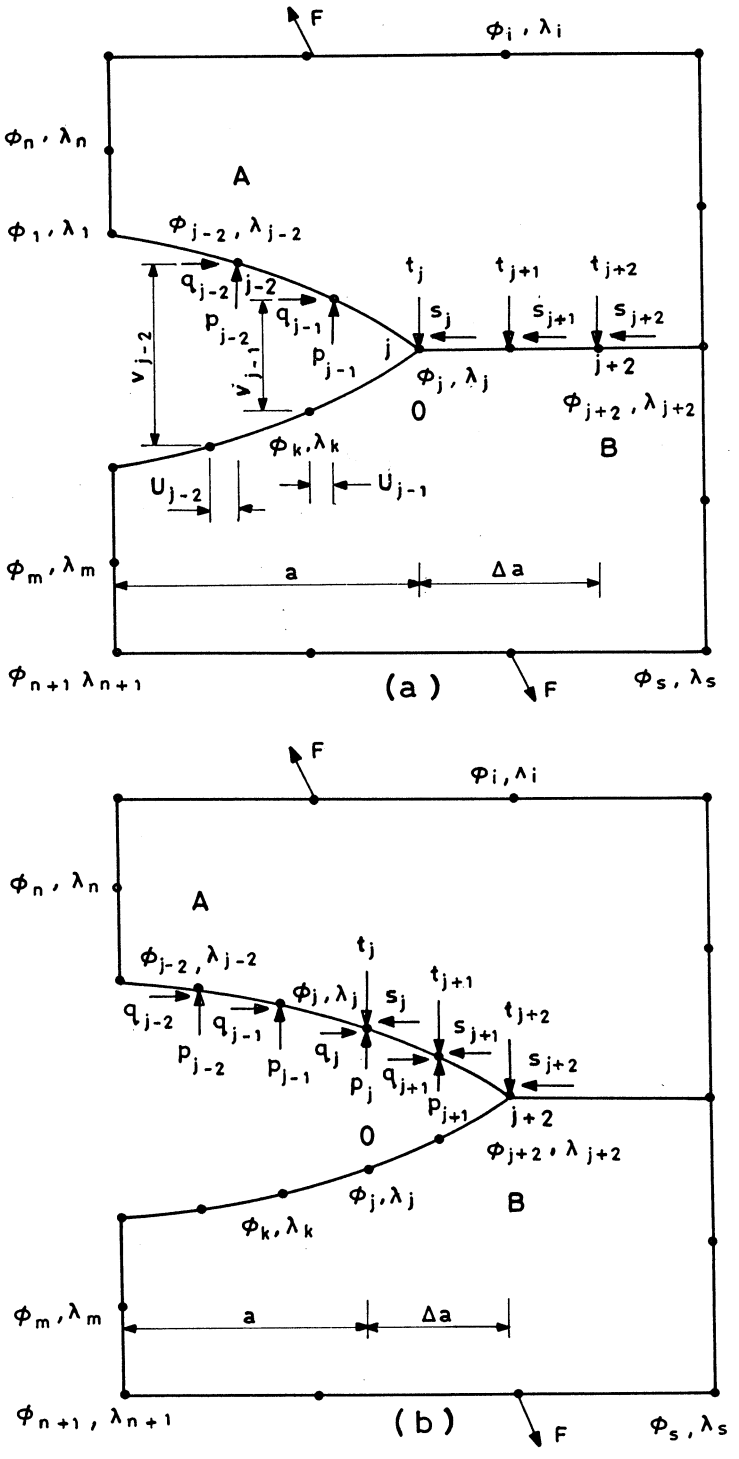

Fig. 2. Illustration of (a) crack under remote and crack edge mechanical loading and thermal field and (b) crack closure forces.

flux conditions on the other as discussed by Prasad et al. (1994, 1996). This method does not require any subdivisioning of a given region and offers some advantages in the study of crack extensions.

After the BE analysis, displacement comparison is commonly employed to evaluate the SIFs. Blandford et al. (1981) and Martinez and Dominguez (1984) have proposed special crack tip elements to include the strain and traction singularities simultaneously and improve the accuracy of results through the displacement comparison. The SIFs can also be computed via the evaluation of J-integrals (Prasad et al., 1994, 1996). Inspired by the success of modified crack closure integral (MCCI) technique for the computation of the SIFs with high accuracy in the finite element method (FEM) (Maiti, 1992a), efforts have been directed recently to exploit the MCCI to evaluate the SIFs through BEM. Farris and Liu (1993), Maiti et al. (1997), Mukhopadhyay et al. (1998a,b) have shown the effectiveness of this method for remote and/or crack edge loaded problems in mode I and mixed mode.

The MCCI based computation of SIFs for thermal and/or mechanical loading is introduced in this paper. For the computation of displacements and tractions the standard BE formulation is employed. The method of calculation of SIFs given here is different from that of Raveendra et al. (1993), Sladek and Sladek (1993) and Katsareas and Anifantis (1995). Raveendra et al. (1993) and Katsareas and Anifantis (1995) have used the methods based on the comparison of displacement and traction, while Sladek and Sladek (1993) have employed a contour integral based evaluation. In this paper, the SIF is determined from the crack closure work done. The crack closure work is computed through the MCCI. 2-D case studies involving thermal and/or mechanical loading in mode I, or mode II, or mixed mode, are presented. In all the cases computations have been performed employing separately linear, quadratic and quarter point elements around the crack tip.

2. Thermoelastic boundary element formulation

In any thermal analysis by the BEM, there are two stages. In the first stage, the potential problem is solved to determine the temperature field. In the second stage, this temperature field is used as input to solve for the distribution of thermal stresses. In this stage, the thermal loading is treated as body forces (Rizzo and Shippy, 1977). The corresponding boundary integral equation (BIE) is as follows.

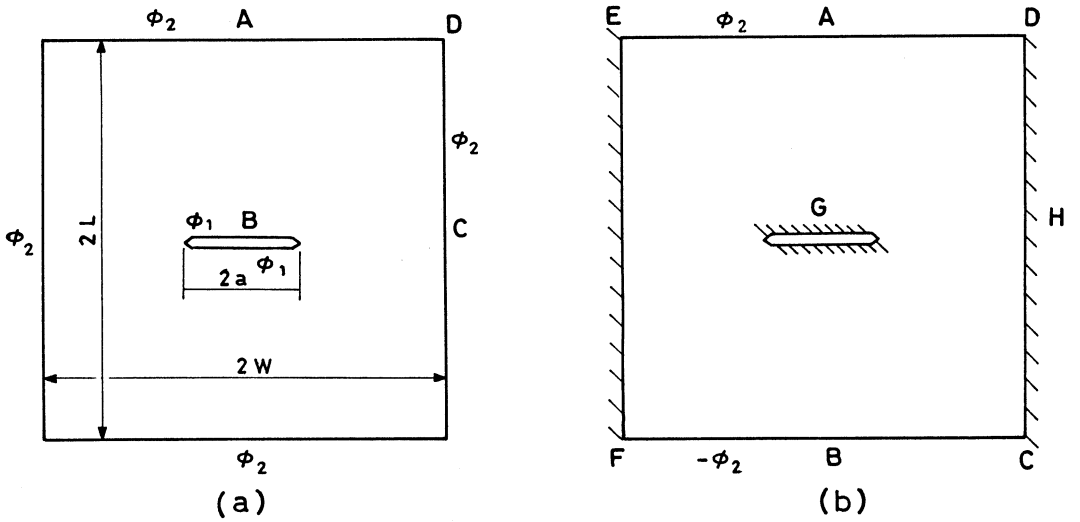

Fig. 3. Centre crack (a) mode I loading (b) mode II loading.

Table 1
Comparison of stress intensity factor (SIF) for mode I centre crack

a/w	SIF (MPa, $\sqrt{}$mm)							
	Sumi and Katayama (1980)	Maiti (1992b)	Present method					
			Linear element		Quadratic element		Quarter point element	
			K_I	% Error[a]	K_I	% Error	K_I	% Error
0.1	0.01739	0.01695	0.01684	−3.143	0.01722	−0.983	0.01670	−3.946
0.2	0.02213	0.02177	0.02139	−3.346	0.02213	−0.013	0.02147	−2.989
0.4	0.02909	0.02799	0.02747	−5.580	0.02867	−1.455	0.02782	−4.380
0.5	0.03099	0.03070	0.02997	−3.277	0.03138	1.242	0.03045	−1.747
0.6	0.03320	0.03294	0.03196	−3.738	0.03356	1.089	0.03257	−1.891

[a] Errors are computed relative to the results of Sumi and Katayama (1980).

$$uLi + \int_S T_{ij} u_j \, dS = \int_S U_{ij} t_j \, dS + \int_V U_{ij} f_j \, dV \quad (1)$$

where S denotes the surface and V is the volume. T_{ij} and U_{ij} are fundamental solutions for traction and displacement and u and t are displacement and traction, respectively. The body force vector f_j can be expressed as gradient of a potential function ϕ.

$$f_j = -\frac{\alpha E}{(1-2\nu)} \frac{\partial \phi}{\partial x_j} \quad (2)$$

where α is the coefficient of thermal expansion, E is elastic modulus and ν is the Poison's ratio. In the event of a variation in temperature within the body an extra term is to be included in the boundary traction.

$$t_j^{tot} = t_j^{mech} + \frac{\alpha E}{(1-2\nu)} \phi n_j \quad (3)$$

where t_j^{tot} is the total traction, t_j^{mech} is the mechanical traction and the last term represents the extra due to temperature field.

Using the Green's second identity, the dimensionality of the second integral on the right hand side can be reduced by one. That is volume integral can be transformed into an area integral and area integral into a line integral.

$$B_i = \int_S M_i \phi \, dS + \int_S N_i \lambda \, dS \quad (4)$$

where M_i and N_i are thermoelastic kernels associated with the temperature and temperature gradient respectively. Here λ denotes the temperature gradient.

3. Computation of SIFS using MCCI

For analysing a mixed mode thermal stress problem through the subregion analysis the domain is to be broken into a convenient number of subregions. At each node of the common interface of the two adjacent regions temperature are the same, and temperature gradients are equal and opposite (Fig. 1a). Similarly the tractions at the common interface nodes are equal and opposite.

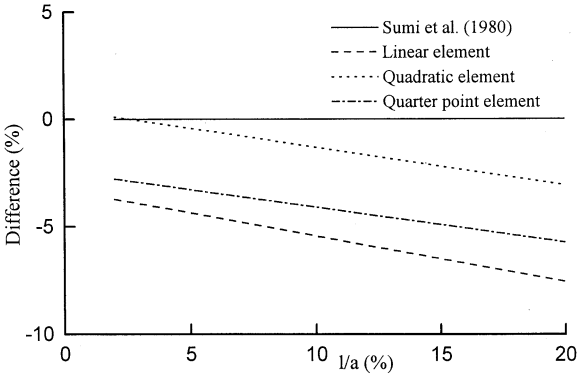

Fig. 4. Effect of crack tip element size on accuracy for centre crack under mode I thermal load.

Table 2
Comparison of stress intensity factor (SIF) correction factor Y for mode II centre crack

a/w	SIF correction factor Y							
	Sumi and Katayama (1980)	Maiti (1992b)	Present method					
			Linear element		Quadratic element		Quarter point element	
			Y	% Error[a]	Y	% Error	Y	% Error
0.1	0.0210	0.0180	0.0188	−10.4366	0.0196	−6.7619	0.0189	−9.7806
0.2	0.0530	0.0540	0.0523	−1.4076	0.0528	−0.3857	0.0511	−3.5502
0.3	0.0940	0.0950	0.0922	−1.9356	0.0937	−0.3121	0.0907	−3.5099
0.4	0.1410	0.1410	0.1357	−3.7236	0.1388	−1.5622	0.1343	−4.7345
0.5	0.1880	0.1900	0.1822	−3.0984	0.1870	−0.5174	0.1810	−3.7065
0.6	0.2470	0.2430	0.2329	−5.7106	0.2402	−2.7510	0.2325	−5.8718

[a] Errors are computed relative to the results of Sumi and Katayama (1980).

The crack edges are loaded by thermal loads. As the crack tip advances from O to B (Fig. 1b), the newly formed crack edges (OB) give way to crack opening but the traction conditions are not changed. Before and after the crack extension the temperatures $(\phi_j, \phi_{j+1}, \phi_{j+2})$ and gradients $(\lambda_j, \lambda_{j+1}, \lambda_{j+2})$ are the same at the nodes j, $j+1$ and $j+2$. Hence the mode I crack closure work for a crack subjected to remote mechanical plus thermal loading is given by the following.

$$W_{\mathrm{I}} = \frac{1}{2}\int_0^l vt \, \mathrm{d}x \tag{5}$$

where l is the crack tip element size, v is the crack opening and t is the traction on the ligament (OB) before the crack extension. The crack closure work for a mode II crack can be calculated in a similar manner.

If a problem involves remote as well as mechanical loading on crack edges/faces, e.g. fluid pressure, on top of any thermal loading (Fig. 2a), as the crack extends up to B, the newly formed crack edges become subjected to the same fluid pressure (Fig. 2b). The newly formed crack edge OB will also be subjected to traction due to thermal loading. The treatment of remote loading and crack edge fluid pressure is the same in the FEM and BEM. In that extra crack closure arises due to the fluid pressure on the newly opened up crack edges. There is however clear difference between FEM (Maiti, 1992a) and BEM in respect of the thermal loading. This thermal traction remains constant throughout the crack opening. The same traction also exists over the span OB when the subregion analysis is done. This, therefore, does not contribute to any additional crack closure work.

Thus, in the case of thermal loading over the whole domain and fluid pressure on the crack edges the crack closure work has two parts. One part is due to the closure forces arising out of thermal loading and fluid pressure and the other is due to crack edge loading p on the extended crack. That is, for a mode I problem

$$W_{\mathrm{I}} = \frac{1}{2}\int_0^l vt \, \mathrm{d}x + \frac{1}{2}\int_0^l vp \, \mathrm{d}x \tag{6}$$

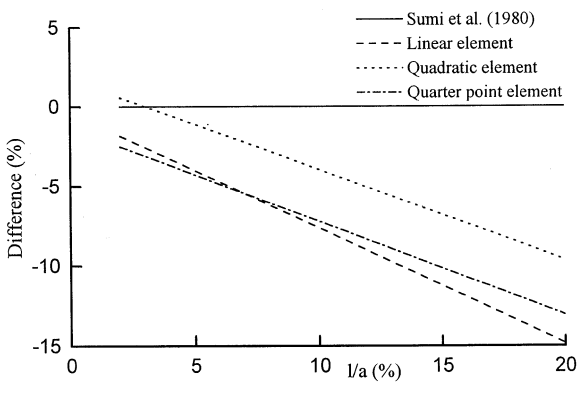

Fig. 5. Effect of crack tip element size on accuracy for centre crack under mode II thermal load.

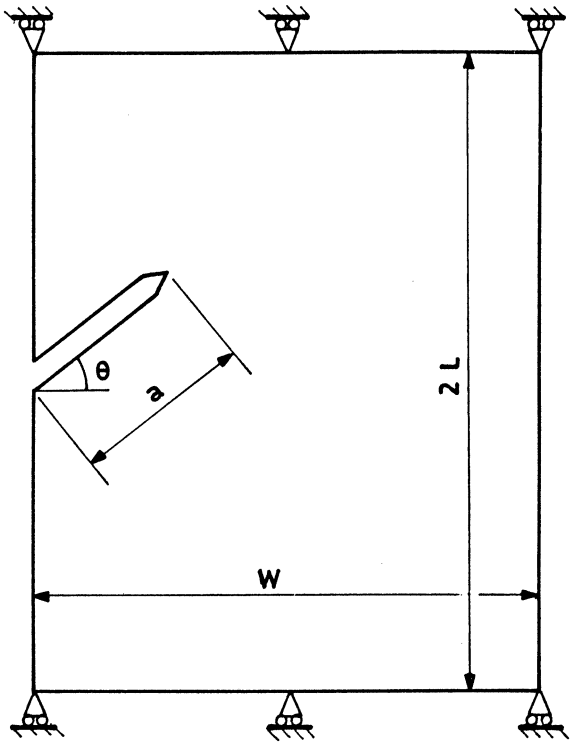

Fig. 6. Slant edge crack.

Similarly for a mode II crack the crack closure work

$$W_{II} = \frac{1}{2}\int_0^l ut\ \mathrm{d}x + \frac{1}{2}\int_0^l us\ \mathrm{d}x \tag{7}$$

where u is the sliding displacement between two crack edges, s is the traction and q is distribution of external shear load on the crack edges.

The energy release rate computations for the boundary element models involving linear, quadratic and quarter point elements in thermal problems can be performed following Mukhopadhyay et al. (1998a,b). The mode I and mode II energy release rates for the linear element are

$$G_I = v_{j-1}(c_1 t_j + c_2 t_{j+1} + c_3 p)/12 \tag{8}$$

$$G_{II} = u_{j-1}(c_1 s_j + c_2 s_{j+1} + c_3 q)/12 \tag{9}$$

where $c_1 = 2$, $c_2 = 1$ and $c_3 = 3$.

For the quadratic element,

$$G_I = [v_{j-1}(c_1 t_j + c_2 t_{j+1} + c_3 t_{j+2} + c_4 p) + v_{j-2}(c_5 t_j + c_6 t_{j+1} + c_7 t_{j+2} + c_8 p)/60] \tag{10}$$

$$G_{II} = [u_{j-1}(c_1 s_j + c_2 s_{j+1} + c_3 s_{j+2} + c_4 q) + u_{j-2}(c_5 s_j + c_6 s_{j+1} + c_7 s_{j+2} + c_8 q)/60] \tag{11}$$

where $c_1 = 2$, $c_2 = 16$, $c_3 = 2$, $c_4 = 20$, $c_5 = 4$, $c_6 = 2$, $c_7 = -1$ and $c_8 = 5$.

For the quarter point element,

$$G_I = [v_{j-1}(c_1 t_j + c_2 t_{j+1} + c_3 t_{j+2} + c_4 p) + v_{j-2}(c_5 t_j + c_6 t_{j+1} + c_7 t_{j+2} + c_8 p)/60] \tag{12}$$

$$G_{II} = [u_{j-1}(c_1 s_j + c_2 s_{j+1} + c_3 s_{j+2} + c_4 q) + u_{j-2}(c_5 s_j + c_6 s_{j+1} + c_7 s_{j+2} + c_8 q)/60] \tag{13}$$

where $c_1 = (140 - 45\pi)$, $c_2 = (60\pi - 176)$, $c_3 = (56 - 15\pi)$, $c_4 = 20$, $c_5 = (11.25\pi - 34)$, $c_6 = (56 - 15\pi)$, $c_7 = (3.75\pi - 12)$ and $c_8 = 10$.

The terms containing p and q vanish in the absence of crack edge mechanical loading. The mode I and mode II SIFs (K_I and K_{II}) can be determined from the standard relationship between G_i and K_i, I = I and II.

4. Case studies

Five case studies, one each on mode I centre cracked plate, mode II centre cracked plate, mixed mode edge crack, pressurised cylinder with radial crack and tee joint with edge crack, is presented. For all the five cases the temperature and temperature gradients are first computed using the standard potential boundary element formulation. In the second stage the stress analysis is done. The plane strain condition has been assumed throughout. The computations are performed on a PC 486 with a single precision arithmetic.

4.1. Centre cracked plate under mode I loading

In this case (Fig. 3a), the crack edge is maintained at a temperature $\phi_1 = 0°C$. The outer edges of the plate is maintained at $\phi_2 = 100°C$. The major dimensions are $W = 40$ mm, $L = 40$ mm.

a/W ratio is varied from 0.1 to 0.6. The material properties are as follows: elastic modulus $E=1$ MPa, Poisson's ratio $v=0.3$, coefficient of thermal expansion $\alpha=10^{-4}$ °C^{-1}. No restraint is applied on the deformation of the plate. Due to symmetry a quarter of the plate ABCD is modelled. The similar nodal arrangements have been considered for linear and quadratic elements. Total number of nodes used is 46. The crack tip element size is 1% for linear and 2% for quadratic and quarter point elements. The computed SIFs are presented in Table 1. The table also includes the results due to Sumi and Katayama (1980). The error indicated in Table 1 is with respect to the solution of Sumi and Katayama (1980). The proposed MCCI scheme gives rise to a maximum error of 5.6, 1.5 and 4.4% for the case of linear, quadratic and quarter point elements respectively.

The dependence of the computed SIFs based on the proposed scheme on the crack tip element size for linear, quadratic and quarter point elements has been examined. The results are presented in Fig. 4. The straightlines are the best fit lines. The l/a is varied from 2 to 20%.

4.2. Centre cracked plate under mode II loading

In this example (Fig. 3b) the top and bottom edges ED and FC are maintained at temperature ϕ_2 and $-\phi_2$, respectively. The edges FE and DC and the crack edges are insulated. The data used are $\phi_2=10$°C, $E=218.4$ GPa, $v=0.3$, $\alpha=1.67\times 10^{-5}$ °C^{-1} and $L/W=1$. a/W ratio is varied from 0.1 to 0.6. The computed SIFs are nondimensionalised dividing by a factor $F=\alpha\phi_2 EW^{0.5}$ so that SIF correction factor $Y=K_{II}/F$. One half of the plate ABCD is modelled. The subregion technique is adapted for the analysis. Each region is discretised by introducing 40 nodes. The crack tip element size is $0.02a$ for the linear element and $0.04a$ for the quadratic and the quarter point elements. The computed SIFs correction factor Y

Table 3
Comparison of stress intensity factor (SIF) for angled edge crack

θ	Mode	SIF (MPa, $\sqrt{}$m)			
		Maiti (1992a)	Element type		
			Linear	Quadratic	Quarter point
$L/W=1$					
0.0	I	58.56	57.88	60.98	59.15
20.0	I	55.28	54.50	57.48	55.77
20.0	II	12.33	12.47	13.07	12.66
30.0	I	51.13	50.34	53.13	51.57
30.0	II	17.46	17.48	18.36	17.79
45.0	I		41.12	43.46	42.23
45.0	II		22.20	23.32	22.62
60.0	I		28.73	30.47	29.66
60.0	II		22.19	23.25	22.55
$L/W=2$					
0.0	I	84.34	82.91	88.46	85.93
20.0	I	78.80	76.94	82.30	79.99
20.0	II	16.10	16.77	17.63	17.10
30.0	I	71.44	69.53	74.47	72.41
30.0	II	22.55	23.23	24.50	23.77
45.0	I		53.38	57.26	55.73
45.0	II		28.43	30.01	29.13
60.0	I		33.48	35.70	34.80
60.0	II		26.98	28.82	27.97

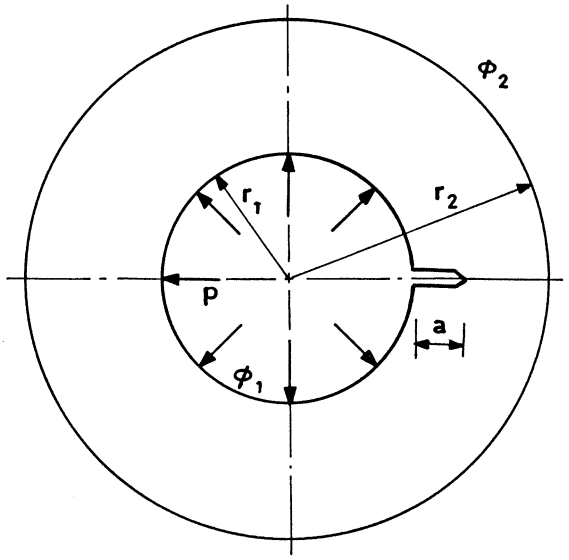

Fig. 7. Pressurised cylinder with radial crack.

is compared with the solution of Sumi and Katayama (1980) as reported by Murakami et al. (1987), in Table 2. The errors are again computed relative to the solutions of Sumi and Katayama (1980). The error is especially high for the case $a/W = 0.1$. Excluding this a/W ratio, the error is within 5.7, 2.8 and 5.9% for the case of linear, quadratic and quarter point elements, respectively.

The effect of crack tip element size on the SIFs for the case of linear, quadratic and quarter point elements is again examined. l/a ratio is varied from 2 to 20%. The results are presented in Fig. 5; the straightlines are the best fit lines.

4.3. Angled edge crack

This is a case involving purely thermal loading. This type of example has been earlier considered by Chen and Chen (1981) and Maiti (1992a). The major dimensions (Fig. 6) are $L/W = 1$ or 2, $W = 20$ mm and $a/W = 0.5$. The crack angle is varied from 0 to 60°. The material data are $E = 2.07 \times 10^5$ MPa, $\nu = 0.3$, and $\alpha = 2.502 \times 10^{-5}$ °C^{-1} (1.39×10^{-5} °F^{-1}). The temperature of the whole body is uniformly reduced by 55.55°C (100°F). The plate movement in the vertical direction at the top and bottom edges is restricted. The whole plate is divided into two subregions. Each subregion is discretised by introducing 40 nodes. The first few elements of the common interface ahead of the crack tip are oriented along the crack line and the remaining are placed horizontally. This facilitates the evaluation of crack closure work using the MCCI technique. The crack tip element size is as usual $0.02a$ for the linear element and $0.04a$ for the quadratic and the quarter point elements. The results are compared with the finite element solutions presented of Maiti (1992a) in Table 3.

4.4. Pressurised cylinder with radial crack

This example involves both thermal and mechanical loading. The outer and inner wall temperatures 300°C and 0°C, respectively. The internal pressure is 10 MPa. The cylinder radii (Fig. 7) are $r_1 = 100$ mm and $r_2 = 200$ mm. The ratio $a/(r_2 - r_1)$ is varied from 0.2 to 0.6. Other data include $E = 2.1 \times 10^5$ MPa, $\nu = 0.3$, $\alpha = 1.2 \times 10^{-5}$ °C^{-1}.

Table 4
Stress intensity factor (SIF) for cylinder with radial crack

$a/(r_2-r_1)$	SIF (MPa, $\sqrt{}$m)		
	Linear element	Quadratic element	Quarter point element
0.2	129.13	132.16	128.19
0.3	135.80	140.22	136.07
0.4	134.46	139.79	135.68
0.5	127.13	133.15	129.25
0.6	114.48	120.86	117.31

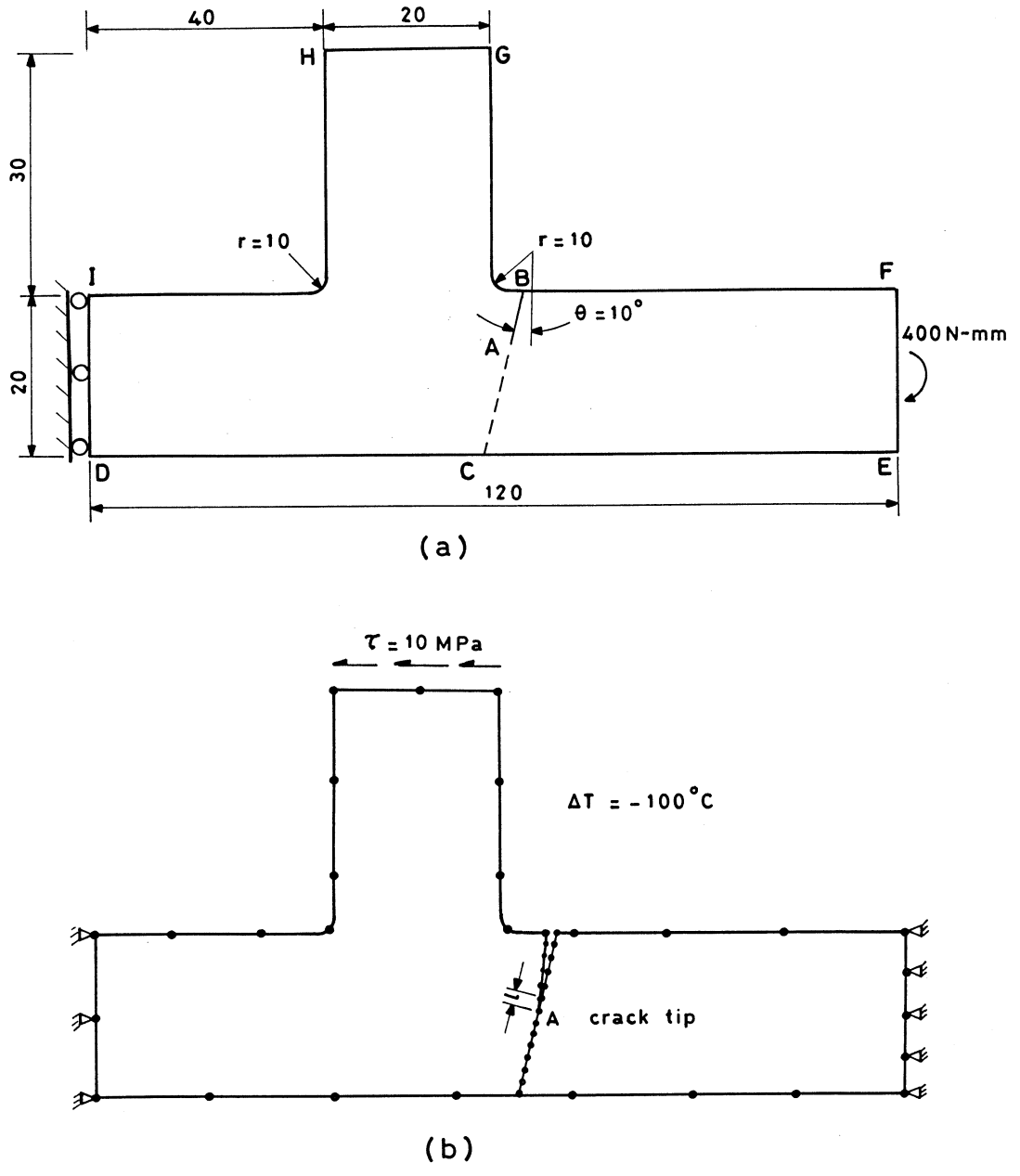

Fig. 8. Tee joint with edge crack (a) pure bending (b) combined thermal and mechanical loading.

One half of the domain is modelled using 76 nodes. The crack tip element size is $0.01a$ when linear elements are employed and it is $0.02a$ when the quadratic and the quarter point elements are employed. Because of symmetry, the condition $\lambda = 0$ holds along the crack line. The computed SIFs for the linear, quadratic and quarter point elements are shown in Table 4. The SIFs have been first compared with a SIF handbook solution (Murakami et al., 1987) considering only internal pressure. There is a good agreement. The maximum difference for the entire range of $a/$

$(r_2 - r_1)$ is 1.2% when quadratic element is used. No data for comparison is available for the SIFs subjected to the combined thermal and mechanical loading (Table 4).

4.5. Tee joint with edge crack

A tee joint with an edge crack subjected to either mechanical or combined thermal and mechanical loading is studied (Fig. 8). The material properties are as follows: $E = 2.1 \times 10^5$ MPa, $\nu = 0.3$, $\alpha = 1.2 \times 10^{-5}$ °C^{-1}. The subregion analysis is employed. Regions IDCABGHI and EFBACE (Fig. 8) are modelled using 31 and 25 quadratic elements, respectively. The crack tip element size is 2% of crack length a. The subsequent elements are $0.04a$, $0.08a$, etc. a/W ratio in the range 0.1–0.5 is examined.

For the tee with an edge crack, the crack propagation direction is 10° off the vertical axis. Watson (1995) analysed a shallow curved crack in mode I. In the present analysis a mixed mode straight crack is considered. To facilitate a comparison with Watson (1995), the case of only mechanical loading is analysed first (Fig. 8a). The computed data on SIF correction factor Y ($Y = K_I/\sigma\sqrt{\pi a}$ or $K_{II}/\sigma\sqrt{\pi a}$) are presented in Table 5. σ is taken as 1 MPa. The mode II SIF is not that significant as the mode I SIF. The mode I SIF results (Table 5) due to bending load agrees well with the solutions presented by Watson (1995).

The thermomechanical case analysed involves a uniform shear load ($\tau = 10$ MPa) on the edge GH and a temperature drop of 100°C keeping the edges ID and EF completely restrained in both x and y directions. The results are presented in Table 6.

5. Discussion

The mode I centre cracked plate problem has also been studied by Maiti (1992b,c) and Prasad et al. (1994). The results of Maiti (1992b) based on a special finite element for variable order singularity is also included in Table 1 for a comparison. The present results are in good agreement with the finite element solutions of Maiti (1992b). The number of nodes employed by him is 191 as against 46 in the present study. In the finite element analysis the crack tip element sizes are in the range 0.833 to 2.5%a (Maiti 1992b). In the present study it is uniformly 2%a. He has reported an error less than 3.8% as against 1.5% in the present case. Maiti (1992c) has again solved this problem employing multicorner variable order singularity finite element where the accuracy is reported to be within 2.1%. The solutions presented by Prasad et al. (1994) which are based on the DBEM, differ by a maximum of 1.23%.

Table 5
Stress intensity factor (SIF) correction factor Y for edge crack in a tee joint under bending load

a/W	Mode	SIF correction factor Y			
		Watson (1995)	Element type		
			Linear	Quadratic	Quarter point
0.1	I	6.8630	6.5946	7.0712	6.8618
0.1	II		0.0029	0.0144	0.0143
0.2	I	6.4160	6.1081	6.6079	6.4187
0.2	II		0.1735	0.1798	0.1749
0.3	I	6.6160	6.1891	6.7949	6.6048
0.3	II		0.3053	0.3129	0.3043
0.4	I	7.2770	6.6467	7.4792	7.2766
0.4	II		0.4178	0.4341	0.4223
0.5	I	8.5140	7.4730	8.7656	8.5389
0.5	II		0.5292	0.5685	0.5533

Table 6
Stress intensity factor (SIF) correction factor Y for edge crack in tee joint under thermal and mechanical loading

a/W	Mode	SIF correction factor Y					
		Only thermal load			Thermal and mechanical load		
		Element type			Element type		
		Linear	Quadratic	QPE[a]	Linear	Quadratic	QPE[a]
0.1	I	487.83	508.06	493.03	537.04	561.03	544.42
0.1	II	15.23	16.86	16.39	11.30	12.99	12.61
0.2	I	476.17	498.04	483.70	518.58	544.08	528.41
0.2	II	33.47	35.63	34.62	28.83	30.89	30.02
0.3	I	489.08	515.34	500.62	526.82	556.70	540.78
0.3	II	43.60	46.11	44.78	38.70	40.99	39.81
0.4	I	503.19	534.25	519.02	536.45	571.02	554.73
0.4	II	48.29	50.97	49.48	43.14	45.52	44.18
0.5	I	505.20	539.55	524.10	533.28	570.83	554.44
0.5	II	48.48	51.43	49.88	43.35	45.47	44.09

[a] QPE, quarter point element.

The centre cracked plate under mode II thermal loading is also solved by Maiti (1992b,c) and Prasad et al. (1994). The solutions presented by Prasad et al. (1994) through the DBEM are also included in Table 2 for a comparison. It may be added here that the results of Prasad et al. (1994) also show a very high difference (14.3%) from the solutions of Sumi and Katayama (1980) for $a/W = 0.1$. The finite element (FE) solutions presented by Maiti (1992b,c) show a maximum difference of 2.7% for the whole range of a/W. The number of nodes used by him is 309 as against 80 in the present study. The crack tip element size is in the range 0.625 to 2%a as compared to 4%a in the present analysis.

In the mixed mode slant edge crack problem, the computed SIFs employing quadratic element is slightly higher than the finite element results of Maiti (1992a). The number of nodes used by Maiti (1992a) is 305 and the crack tip element size is 2%a as compared to the present analysis with 80 nodes and a crack tip element size of 4%a.

For the case of pressurised cylinder with a radial crack (Table 4), the variation of computed SIFs for the combined pressure and thermal loading with $a/(r_2 - r_1)$ shows an initial increase followed by a reversal in the trend. The contribution of internal pressure on the SIF increases with increase in $a/(r_2 - r_1)$ (Mukhopadhyay et al., 1998b). But the thermal load contribution more than nullify this effect after a certain level. As a result the SIF is decreasing as the ratio $a/(r_2 - r_1)$ is exceeding 0.3.

For the tee with an edge crack under thermal loading and combined thermal and shear loading, no data for comparison are available in the literature. The results (Table 5) show that the mode I SIF correction factor Y initially decreases up to $a/W = 0.2$ and then increases when only thermal loading is considered. The mode II effect in this case steadily increases with a/W. The trend is similar when the combined thermal and mechanical loading is considered. The effect of mechanical loading is small compared to the thermal loading. The mode II SIF is again insignificant compared with the mode I SIFs.

The computed SIFs based on the proposed formulation is not very sensitive to the crack tip element size (Figs. 4 and 5). In both the cases the error is within 7.5% for linear element, 4% for quadratic element and 7% for quarter point element with a crack tip element size up to 0.1a. It must be emphasised here that the SIF calculations

based on the displacement comparison are very sensitive to the crack tip element size (Mukhopadhyay et al., 1998a).

6. Conclusion

The MCCI technique is introduced for calculating stress intensity factors in 2-D thermal crack problems based on the boundary element method. A formulation has been proposed to compute SIFs for thermal loading on a crack using the MCCI technique. Mode I, mode II and mixed mode examples under thermal and/or mechanical loading have been considered to demonstrate the accuracy and effectiveness of the scheme. The agreement with the available solution is generally good; the difference is usually less than 2% when quadratic elements are employed. The accuracy of the SIFs evaluated through the MCCI technique is less sensitive to the crack tip element size than the displacement method. A size of the crack tip element of some 6–8% of crack length can be utilised to achieve an accuracy of around 3–5% using either quadratic or quarter point element.

Appendix A. Nomenclature

a	crack length
c_n	coefficients of traction in MCCI formulation
E	elastic modulus
G_{I}, G_{II}	strain energy release rate in mode I, mode II
K_{I}, K_{II}	stress intensity factors
l	crack tip element length
L, W	domain geometric dimensions
p, q	components of crack edge loading normal and parallel to crack
r_1, r_2	internal and external radii
s_j, t_j	components of traction parallel and normal to crack
u, v	components of displacement parallel and normal to crack
W_{I}, W_{II}	crack closure work
x, y	Cartesian co-ordinates
Y	SIF correction factor

Greeks

θ	crack orientation with x-axis
ν	Poisson's ratio
ξ	natural co-ordinate
α	coefficient of thermal expansion
ϕ	potential/temperature
λ	potential/temperature gradient

References

Blandford, G.E., Ingrafea, A.R., Ligget, J.A., 1981. Two-dimensional stress intensity factor computations using the boundary element method. Int. J. Numer. Methods Eng. 17, 387–404.

Chen, W.H., Chen, K.T., 1981. On the study of mixed mode thermal fracture using modified J_{K} integrals. Int. J. Fracture 17, R99–R103.

Farris, T.N., Liu, M., 1993. Boundary element crack closure calculation of three-dimensional stress intensity factors. Int. J. Fracture 60, 33–47.

Katsareas, D.E., Anifantis, N.K., 1995. On the computation of mode I and II thermal shock stress intensity factors using a boundary-only element method. Int. J. Numer. Methods Eng. 38, 4157–4169.

Lee, K.Y., Cho, Y.H., 1990. Boundary element analysis of thermal stress intensity factors for CUSP cracks. Eng. Fract. Mech. 37, 787–798.

Maiti, S.K., 1992a. Finite element computation of crack closure integrals and stress intensity factors. Eng. Fract. Mech. 41, 339–348.

Maiti, S.K., 1992b. A finite element for variable order singularities based on the displacement formulation. Int. J. Numer. Methods Eng. 33, 1955–1974.

Maiti, S.K., 1992c. A multicorner variable order singularity triangle to model neighbouring singularities. Int. J. Numer. Methods Eng. 35, 391–408.

Maiti, S.K., Mukhopadhyay, N.K., Kakodkar, A., 1997. Boundary element method based computation of stress intensity factor by modified crack closure integral. Comput. Mech. 18, 203–210.

Martinez, J., Dominguez, J., 1984. On the use of quarter-point boundary elements for stress intensity factor computations. Int. J. Numer. Methods Eng. 20, 1941–1950.

Mukhopadhyay, N.K., Maiti, S.K., Kakodkar, A., 1998a. Further considerations in modified crack closure integral based computation of stress intensity factor in BEM. Eng. Fract. Mech., 59, 269–279.

Mukhopadhyay, N.K., Maiti, S.K., Kakodkar, A., 1998b. BEM based evaluation of SIFs using modified crack closure integral technique under remote and/or crack edge loading. Eng. Fract. Mech., 61, 655–671.

Murakami, Y., et al. (Eds.), 1987. Stress Intensity Factor Handbook, Pergamon Press, Oxford.

Portela, A., Aliabadi, M.H., Rooke, D.P., 1992. The dual boundary element method: effective implementation for crack problems. Int. J. Numer. Methods Eng. 33, 1269–1287.

Prasad, N.N.V., Aliabadi, M.H., Rooke, D.P., 1994. The dual boundary element method for thermoelastic crack problems. Int. J. Fract. 66, 255–272.

Prasad, N.N.V., Aliabadi, M.H., Rooke, D.P., 1996. Effect of thermal singularities on stress intensity factors: edge crack in rectangular and circular plate. Theoret. Appl. Fracture Mech. 24, 203–215.

Raveendra, S.T., Banerjee, P.K., 1992. Boundary element analysis of cracks in thermally stressed planar structures. Int. J. Solids Struct. 29, 2301–2317.

Raveendra, S.T., Banerjee, P.K., Dargush, G.F., 1993. Three-dimensional analysis of thermally loaded cracks. Int. J. Numer. Methods Eng. 36, 1909–1926.

Rizzo, F.J., Shippy, D.J., 1977. An advanced boundary integral equation method for three-dimensional thermoelasticity. Int. J. Numer. Methods Eng. 11, 1753–1768.

Sladek, V., Sladek, J., 1993. Boundary integral representation of stress intensity factors in thermoelasticity. Eng. Anal. Boundary Elements 12, 127–135.

Sladek, J., Sladek, V., 1997. Computation of thermoelastoplastic stresses in crack problems by the BEM. Int. J. Fracture 83, 359–378.

Sumi, N., Katayama, T., 1980. Thermal stress singularities at tips of a Griffith crack in a finite rectangular plate. Nucl. Eng. Des. 60, 389–394.

Watson, J.O., 1995. Singular boundary elements for the analysis of cracks in plane strain. Int. J. Numer. Methods Eng. 38, 2389–2411.